

# A multiscale, finite deformation formulation for surface stress effects on the coupled thermomechanical behavior of nanomaterials

Geng Yun, Harold S. Park \*

*Department of Civil and Environmental Engineering, Vanderbilt University, Nashville, TN 37235, United States*

Received 24 August 2007; received in revised form 17 December 2007; accepted 1 February 2008

Available online 14 February 2008

## Abstract

We present a multiscale, finite deformation formulation that accounts for surface stress effects on the coupled thermomechanical behavior and properties of nanomaterials. The foundation of the work lies in the development of a multiscale surface Helmholtz free energy, which is constructed through utilization of the surface Cauchy–Born hypothesis. By doing so, temperature-dependent surface stress measures as well as a novel form of the heat equation are obtained directly from the surface free energy. The development of temperature-dependent surface stresses distinguishes the present approach, as the method can be utilized to study the behavior of nanomaterials by capturing the size-dependent variations in the thermoelastic properties with decreasing nanostructure size. The coupled heat and momentum equations are solved in 1D using a fully implicit, monolithic scheme, and show the importance of capturing surface stress effects in accurately modeling the thermomechanical behavior of nanoscale materials.

© 2008 Elsevier B.V. All rights reserved.

*Keywords:* Surface Cauchy–Born; Thermomechanical coupling; Helmholtz free energy; Local harmonic approximation; Surface stress

## 1. Introduction

Nanomaterials such as nanowires have been studied intensely in recent years due to their unique and often superior mechanical, electrical and optical properties that arise because of their nanometer size scale [1–3]. Because of these unique properties, nanowires will be utilized as structural materials, bio-sensors, force and mass detectors, as circuitry and interconnects in future nanoscale devices, and as the basic building blocks of nanoelectromechanical systems (NEMS) [4–9].

The physical properties of nanowires are fundamentally different from those of the corresponding bulk materials because of the dominant influence of nanoscale free surfaces; free surface effects impact all physical properties of nanowires, including their mechanical [10], optical [11] and thermal [12,13] properties. In the case of the thermal and optical properties, the small cross-section of the nano-

wires induces strong quantum confinement effects which cause a large variance in those properties, for example the coefficient of thermal expansion or the optical bandgap, at nanometer length scales.

For mechanical and elastic properties, nanoscale free surface effects such as surface stresses [14] arise because surface atoms have a different bonding environment than atoms that lie within the material bulk; therefore, the elastic properties of surfaces differ from those of the bulk material, and the effects of the difference between surface and bulk elastic properties on the effective elastic properties of the nanowire become magnified with decreasing structural size and increasing surface area to volume ratio [10,15–20].

A large number of analytic models for the size-dependent elastic properties of nanomaterials have been recently developed [21–28]. Generally, these are enhanced continuum models that use a bulk/surface decomposition to study surface effects with varying nanostructure size. Due to assumptions utilized to make the analyses tractable, the coupled effects of geometry, surface area to volume ratio and system size on the mechanical properties of nanowires have not

\* Corresponding author. Tel.: +1 303 492 7750.

E-mail address: [harold.park@colorado.edu](mailto:harold.park@colorado.edu) (H.S. Park).

been quantified, nor have surface stress effects arising directly from atomistic principles been included in the analyses, which are generally in two-dimensions.

Similarly, a large number of multiscale computational models for studying the properties of nanomaterials through various approaches to atomistic/continuum coupling have been recently developed [29–38]. However, with few exceptions [31,39–43], these methods are incapable of capturing atomic-scale surface stress effects; furthermore, the inclusion of thermal effects in multiscale modeling of nanomaterials, with limited exceptions [44–47], has also been rarely studied, while dissipative effects have also rarely been considered [46].

In the present work, we develop a multiscale, finite deformation formulation to study the coupled thermomechanical behavior of nanomaterials. The approach is grounded through development of a multiscale Helmholtz free energy, where the Helmholtz free energy is made multiscale through utilization of the Cauchy–Born hypothesis [29]. The starting point of the approach is thus identical to that of Xiao et al. [44,45], Liu and Li [46] and Tang et al. [47,48], who developed a multiscale Helmholtz free energy based on the Cauchy–Born approximation.

Upon development of the multiscale Helmholtz free energy, the present work deviates from that of previous work [44–46]. In particular, we incorporate thermally-dependent nanoscale free surface effects into the standard energy equation through development of a surface Helmholtz free energy function. By doing so, the resulting energy equation that contains the size-dependent nanoscale thermal effects can be coupled with a mechanical model, the surface Cauchy–Born model of Park et al. [40,41], which results, for the first time, in a coupled thermomechanical system of equations that naturally captures the size-dependent variations in the thermoelastic properties due to nanoscale free surface effects. These free surface effects are captured because the surface Helmholtz free energies accurately model the variation in the thermoelastic properties of surface atoms due to their reduced number of bonding neighbors as compared to bulk atoms, and lead to size-dependence in the elastic modulus and coefficient of thermal expansion, which is critical in the analysis of nanomaterials [13].

We also solve the coupled heat and momentum equations using a fully implicit monolithic scheme [49] after discretization of the governing equations using a Galerkin finite element approximation. A simple 1D numerical example is presented that illustrates the importance of accurately capturing nanoscale surface stress effects in modeling the dynamic, thermomechanical behavior of nanoscale materials.

## 2. Multiscale finite temperature modeling

### 2.1. Overview of Cauchy–Born theory

The Cauchy–Born (CB) hypothesis is based on Green elastic theory, in which continuum stress and moduli are

derived assuming the existence of a strain energy density function  $\Phi$ . In order to satisfy material frame indifference, the strain energy density  $\Phi$  must be expressed as a function of the right stretch tensor  $\mathbf{C}$ , i.e.  $\Phi(\mathbf{C})$ , where  $\mathbf{C} = \mathbf{F}^T \mathbf{F}$  and  $\mathbf{F}$  is the continuum deformation gradient.

The foundation of CB modeling is based upon creating a link between atomistics and continua; to enable this link, a strain energy density can be constructed for crystalline materials by considering the bonds in a representative volume of the crystal [29,50]. For the case of a centrosymmetric crystal modeled using only pair interactions, the strain energy density is defined in terms of the interatomic potential  $U$  as [50]

$$\Phi(\mathbf{C}) = \frac{1}{2} \frac{1}{\Omega_0} \sum_{i=1}^{n_b} U(r^{(i)}(\mathbf{C})). \quad (1)$$

In (1),  $n_b$  is the total number of bonds to a representative bulk atom,  $\Omega_0$  is the representative atomic volume in the undeformed configuration and  $r^{(i)}$  is the deformed bond length, which follows the relationship

$$r^{(i)} = \sqrt{\mathbf{R}_0 \cdot \mathbf{C} \mathbf{R}_0^{(i)}}, \quad (2)$$

where  $\mathbf{R}_0$  is the undeformed bond vector. From the strain energy density given in (1), one can obtain standard continuum stress measures such as the second Piola–Kirchhoff (PK2) stress ( $\mathbf{S}$ ) as

$$\mathbf{S}(\mathbf{C}) = 2 \frac{\partial \Phi(\mathbf{C})}{\partial \mathbf{C}} = \frac{1}{\Omega_0} \sum_{i=1}^{n_b} \left( U'(r^{(i)}) \frac{\partial r^{(i)}}{\partial \mathbf{C}} \right). \quad (3)$$

Depending on the stress measure that is desired, the first Piola–Kirchhoff (PK1) stress  $\mathbf{P}$  can be found through the relationship  $\mathbf{P} = \mathbf{S} \mathbf{F}^T$ .

The strain energy density (1) is exact in describing the change in energy per volume of a bulk atom in a corresponding defect-free atomistic system subject to homogeneous deformation. Furthermore, the continuum stress measure in (3) is derived using atomistic information; thus the CB hypothesis is said to be hierarchically multiscale in nature. We note that the CB model can also be utilized in conjunction with more complicated interatomic interactions such as embedded atom (EAM) potentials [29,41,42,51] for FCC metals, Tersoff-type potentials for silicon [47,52,53], or carbon nanotubes [54,55].

There are two major assumptions underlying the CB hypothesis. The first is that, as mentioned above, the underlying atomistic system is constrained to deform homogeneously according to the stretch tensor  $\mathbf{C}$ . This restriction can be relaxed to accommodate lattice defects or material plasticity through development of the quasi-continuum, or non-local CB model [29]. The second major assumption is that all points at which the Cauchy–Born hypothesis is applied are assumed to lie in the bulk because  $\Phi(\mathbf{C})$  does not account for surface effects. Therefore, in order to capture nanoscale free surface effects such as surface stresses, we will, in a later section, augment the bulk

energy density in (1) with a surface energy density which accounts for the non-bulk potential energy that atoms lying along the surfaces of a body exhibit [40–43].

## 2.2. Multiscale Helmholtz free energy

The goals of this section are to develop a heat equation that is valid at the nanoscale along with continuum stress measures that are temperature-dependent and derived from atomistic principles. To derive both of these, we introduce the Helmholtz free energy [56], which can be written as

$$A_0 = U + k_B T \sum_j \ln \left( 2 \sinh \left( \frac{\bar{h} \omega_j}{2k_B T} \right) \right), \quad (4)$$

where  $h$  is Planck's constant, where  $\bar{h} = h/2\pi$ ,  $\omega_j$  is the vibrational frequency,  $j$  includes all the non-zero vibrational modes of the system,  $T$  is the temperature,  $U$  is the potential energy and  $k_B$  is the Boltzmann coefficient.

Because of the computational expense required to evaluate the individual vibrational frequencies  $\omega_j$  for all atoms in the system, LeSar et al. developed the local harmonic approximation (LHA) [57], in which the atomic vibrational frequencies are decoupled from each other, leading to the modified Helmholtz free energy

$$A_0 = U + nk_B T \sum_{i=1}^{na} \ln \left( \frac{h\bar{D}^{1/2n}}{2\pi k_B T} \right), \quad (5)$$

where  $na$  is the total number of atoms in the system,  $n$  is the number of degrees of freedom for each atom and  $\bar{D}$  is the determinant of the  $n \times n$  dynamical matrix  $D$ , which can be written as

$$D_{ij} = \frac{1}{m} \frac{\partial^2 U}{\partial x_i \partial x_j}, \quad (6)$$

where  $m$  is the mass of atom  $i$ .

The LHA approximation is made during the calculation of the dynamical matrix  $D$ ; it is made by neglecting the off diagonal terms that couple the vibrational modes of different atoms in the system. Thus, the resulting diagonalization of  $D$  makes the approximation harmonic, in that the modes of vibration are independent of the neighboring atoms. The LHA has been carefully evaluated by various researchers [48,56,58–60]; generally, the consensus has been that the LHA is valid up to about one half the melt temperature for a given material, though that value can change depending on the anharmonicity of the interatomic potential.

At this point, the Helmholtz free energy in (5) is still exclusively in terms of atomistic degrees of freedom; to make the free energy multiscale, we apply the CB hypothesis [29] following previous approaches [44–47] to arrive at the multiscale Helmholtz free energy density

$$\frac{A_0(\mathbf{C})}{\Omega_0} = \Phi(\mathbf{C}) + \frac{nk_B T}{\Omega_0} \sum_{i=1}^{na} \ln \left( \frac{h\bar{D}^{1/2n}(\mathbf{C})}{2\pi k_B T} \right), \quad (7)$$

where  $\Phi(\mathbf{C})$  is the strain energy density previously defined in (1) and  $\bar{D}$  is the determinant of the dynamical matrix  $D$ . We can rewrite (7) as

$$\rho_0 \Psi = \Phi(\mathbf{C}) + nk_B \rho_v T \ln \left( \frac{h\bar{D}^{1/2n}(\mathbf{C})}{2\pi k_B T} \right), \quad (8)$$

where  $\rho_0$  is the mass density in the undeformed configuration,  $\Psi$  is the Helmholtz free energy per unit mass and  $\rho_v$  is the number of atoms per unit volume in the undeformed configuration.

The importance of deriving the multiscale Helmholtz free energy in (8) is that we can, using standard continuum mechanics arguments (for example in (3)), derive the stress and modulus, as well as the governing energy equation.

## 2.3. Thermomechanical stress measures

In the present work, we utilize the Lennard–Jones (LJ) 6–12 potential energy and assume second nearest neighbor atomic interactions; the LJ potential can be written as

$$U(r) = 4\epsilon \left( \left( \frac{\sigma}{r} \right)^{12} - \left( \frac{\sigma}{r} \right)^6 \right), \quad (9)$$

where  $\epsilon$  has units of energy and  $\sigma$  has units of length. Furthermore, because the multiscale Helmholtz free energy in (8) is written in terms of the stretch tensor  $\mathbf{C}$ , we can derive the PK2 stress  $\mathbf{S}$  by following the relation:

$$\mathbf{S} = 2 \frac{\partial(\rho_0 \Psi)}{\partial \mathbf{C}}. \quad (10)$$

In applying (10), we find that the PK2 stress has both mechanical and thermal components. In particular, the mechanical part of the PK2 stress  $\mathbf{S}_m$  can be written as

$$\mathbf{S}_m = 2 \frac{\partial \Phi(\mathbf{C})}{\partial \mathbf{C}} = \frac{1}{\Omega_0} \sum_{i=1}^{n_b} \left( U'(r^{(i)}) \frac{\partial r^{(i)}}{\partial \mathbf{C}} \right), \quad (11)$$

while the thermal part of the PK2 stress is obtained by

$$\mathbf{S}_t = 2 \frac{\partial}{\partial \mathbf{C}} \left( nk_B \rho_v T \ln \left( \frac{h\bar{D}^{1/2n}(\mathbf{C})}{2\pi k_B T} \right) \right) = \frac{k_B \rho_v T}{\bar{D}} \frac{\partial \bar{D}}{\partial \mathbf{C}}. \quad (12)$$

Because they also began with a Helmholtz free energy based on the CB model, similar expressions were derived by Xiao et al. [44,45], Liu and Li [46] and Tang et al. [47,48].

## 2.4. Heat equation derivation

Once the Helmholtz free energy is known as in (8), the governing heat equation for coupled finite deformation thermoelasticity can be derived using the Helmholtz free energy following Parkus [61] as

$$-\frac{\partial}{\partial X_A} \left( k J F_{Ai}^{-1} F_{Bi}^{-1} \frac{\partial T}{\partial X_B} \right) = \rho_0 T \left( \frac{\partial^2 \Psi}{\partial T \partial E_{AB}} \dot{E}_{AB} + \frac{\partial^2 \Psi}{\partial T^2} \dot{T} \right), \quad (13)$$

where  $k$  is the thermal conductivity,  $J$  is the determinant of  $\mathbf{F}$  and  $E_{AB}$  are the components of Green strain tensor  $\mathbf{E}$ . Enforcing mass conservation requires that  $\rho J = \rho_0$  with  $\rho$  being the mass density in the deformed configuration, while all heat sources have been ignored. We note the assumption of the Fourier heat conduction law in obtaining (13).

We introduce the relationships

$$\dot{E}_{AB} = \frac{1}{2}(\dot{F}_{iA}F_{iB} + F_{iA}\dot{F}_{iB}), \quad (14)$$

and

$$\frac{\partial^2 \Psi}{\partial T \partial E_{AB}} \dot{E}_{AB} = \frac{1}{2} \frac{\partial^2 \Psi}{\partial T \partial F_{iA}} F_{Bi}^{-1} (\dot{F}_{jA}F_{jB} + F_{jA}\dot{F}_{jB}), \quad (15)$$

which allow us to rewrite (13) giving a general heat equation as

$$\begin{aligned} & -\frac{\partial}{\partial X_A} \left( k J F_{Ai}^{-1} F_{Bi}^{-1} \frac{\partial T}{\partial X_B} \right) \\ & = \rho_0 T \left( \frac{1}{2} \frac{\partial^2 \Psi}{\partial T \partial F_{iA}} F_{Bi}^{-1} (\dot{F}_{jA}F_{jB} + F_{jA}\dot{F}_{jB}) + \frac{\partial^2 \Psi}{\partial T^2} \dot{T} \right). \end{aligned} \quad (16)$$

We make three comments here. First, no assumption as to the form of the Helmholtz free energy  $\Psi$  or the atomistic potential energy  $U$  have been made in deriving (16). Second, Eq. (16) has been in existence for many years, for example Eq. (5.28) in Parkus [61]. Finally, thermoelastic dissipation which occurs due to the change in mechanical deformation, i.e. the  $\dot{F}$  terms in (16), are fully accounted for.

Continuing forward with our derivation, we now make assumptions as to the particular form of the Helmholtz free energy and the potential energy by utilizing the LJ 6–12 potential described in (9) to rewrite (8) as

$$\rho_0 \Psi = W_1(\mathbf{F}) + T W_2(\mathbf{F}) - C_1 T \ln(T), \quad (17)$$

where

$$W_1(\mathbf{F}) = \Phi(\mathbf{C}), \quad (18)$$

$$C_1 = n k_B \rho_v, \quad (19)$$

and

$$W_2(\mathbf{F}) = C_1 \ln \left( \frac{h(\bar{D}(\mathbf{F}))^{1/2n}}{2\pi k_B} \right). \quad (20)$$

As a result, the general 3D form of the modified heat equation (16) can be written as, for the LJ 6–12 potential with second nearest neighbor interactions

$$\begin{aligned} & -\frac{\partial}{\partial X_A} \left( k J F_{Ai}^{-1} F_{Bi}^{-1} \frac{\partial T}{\partial X_B} \right) \\ & = \frac{1}{2} T \left( \frac{\partial W_2(\mathbf{F})}{\partial F_{iA}} F_{Bi}^{-1} + \frac{\partial W_2(\mathbf{F})}{\partial F_{iB}} F_{Ai}^{-1} \right) F_{jB} \dot{F}_{jA} - C_1 \dot{T}. \end{aligned} \quad (21)$$

In the present work, the focus is on developing our ideas in 1D, so we now proceed to derive the specific 1D form of (21).

## 2.5. Remarks on the assumption of linear thermoelasticity

At this juncture, due to the complex nature of the general nonlinear heat equation given in (16), various simplifications can be made. A common assumption is that of a linear thermoelastic constitutive relationship [49], for example

$$\mathbf{S} = \mathcal{C} \mathbf{E} - \frac{Y\alpha}{1-\nu} \Theta \mathbf{I}, \quad (22)$$

where  $\mathbf{I}$  is the identity tensor,  $\mathcal{C}$  is the material tensor,  $\mathbf{E}$  is the Green strain tensor,  $Y$  is the Young's modulus,  $\nu$  is the Poisson's ratio,  $\alpha$  is the coefficient of thermal expansion and  $\Theta = T - T_0$ . Using this, the modified form of the heat equation in (16) is given as [49]

$$\nabla \cdot \mathbf{h} = \frac{Y\alpha}{1-\nu} T \dot{\epsilon} + \rho C_p \dot{T}, \quad (23)$$

where  $\dot{\epsilon}$  is the time derivative of the sum of the diagonal components of  $\mathbf{E}$ ,  $C_p$  is the heat capacity,  $\mathbf{h}$  is the heat flux vector in the undeformed configuration, where the heat flux vector  $\mathbf{h}$  can be mapped back to the deformed configuration via the relationship  $\mathbf{h} = \mathbf{J} \mathbf{F}^{-1} \mathbf{q}$ , where  $\mathbf{q}$  is the heat flux vector in the deformed configuration.

Note that, due to the assumption of linearity in (22) and (23), all the material properties are *constant*, and thus are not size-dependent, which makes the assumption of linearity invalid for the analysis of nanomaterials. Exceptions to the assumption of material linearity can be found in the work of Xiao et al. [44,45], Liu and Li [46] and Tang et al. [47,48] through the development of the multiscale Helmholtz free energy using the Cauchy–Born hypothesis. However, we are aware of no work that has accounted for surface effects and thus the size-dependence of the material properties of nanomaterials.

## 2.6. 1D heat equation

In evaluating (7) for a 1D chain of atoms,  $\Omega_0 = \frac{1}{4} h a^3$ , where  $h a$  is the undeformed bond length,  $\rho_v = \frac{4}{h a^3}$ , and  $n = 1$ , which enables us to obtain an analytic expression for the strain energy density  $\Phi$  assuming the LJ 6–12 potential in (9) with second nearest neighbor atomic interactions as

$$\Phi = \frac{16\epsilon}{h a^3} \left( \left( 1 + \frac{1}{2^{12}} \right) \frac{\sigma^{12}}{h a^{12}} \frac{1}{F^{12}} - \left( 1 + \frac{1}{2^6} \right) \frac{\sigma^6}{h a^6} \frac{1}{F^6} \right), \quad (24)$$

where  $F$  is the deformation gradient in 1D. The determinant of the local dynamic matrix is also found analytically to be

$$\bar{D}(F) = \frac{8\epsilon}{m} \left( \left( 1 + \frac{1}{2^{14}} \right) \frac{156\sigma^{12}}{h a^{14}} \frac{1}{F^{14}} - \left( 1 + \frac{1}{2^8} \right) \frac{42\sigma^6}{h a^8} \frac{1}{F^8} \right). \quad (25)$$

For simplicity, we introduce several constants

$$A = \left(1 + \frac{1}{2^{12}}\right) \frac{16\epsilon}{ha^3} \frac{\sigma^{12}}{ha^{12}}, \tag{26}$$

$$B = -\left(1 + \frac{1}{2^6}\right) \frac{16\epsilon}{ha^3} \frac{\sigma^6}{ha^6}, \tag{27}$$

$$R = \frac{4k_B}{ha^3} \ln\left(\frac{h}{2\pi k_B} \left(\frac{8\epsilon}{m}\right)^{1/2}\right), \tag{28}$$

$$D = \left(1 + \frac{1}{2^{14}}\right) \frac{156\sigma^{12}}{ha^{14}}, \tag{29}$$

$$E = -\left(1 + \frac{1}{2^8}\right) \frac{42\sigma^6}{ha^8}, \tag{30}$$

so that we can express the Helmholtz free energy density as

$$\rho_0 \Psi = \frac{A}{F^{12}} + \frac{B}{F^6} + RT - \frac{4k_B}{ha^3} T \ln T + \frac{4k_B}{ha^3} T \ln\left(\left(\frac{D}{F^{14}} + \frac{E}{F^8}\right)^{1/2}\right). \tag{31}$$

From (31), we obtain the PK1 stress as

$$P = -\frac{12A}{F^{13}} - \frac{6B}{F^7} - \frac{4k_B}{ha^3} \left(\frac{7D + 4E \cdot F^6}{D \cdot F + E \cdot F^7}\right) T. \tag{32}$$

By substituting (31) into (13) and differentiating, we obtain the following 1D heat equation:

$$\frac{4k_B}{ha^3} \dot{T} - k \frac{\partial}{\partial X} \left(\frac{1}{F} \frac{\partial T}{\partial X}\right) + \frac{4k_B}{ha^3} \left(\frac{7D + 4E \cdot F^6}{D \cdot F + E \cdot F^7}\right) T \dot{F} = 0. \tag{33}$$

We emphasize again that Eq. (33) is important because: (1) aside from the assumption of Fourier heat conduction, the material properties are not constant, and depend on temperature, size and deformation. (2) Eq. (33) is dissipative, which is key to modeling thermoelastic dissipation in nanomaterials [49,62,63]. (3) Eq. (33) is nonlinearly coupled to the momentum equation through the deformation gradient  $F$  as well as its time rate of change  $\dot{F}$ , and thus is valid for finite deformations.

### 3. Coupled heat/momentum equations and weak forms

#### 3.1. Momentum equation weak form

The 1D momentum equation is

$$\rho_0 \ddot{u} = \frac{dP_m}{dX} + \frac{dP_t}{dX}, \tag{34}$$

where body forces and velocity-dependent damping have been ignored,  $P_m$  is the mechanical part of the first Piola–Kirchoff stress from (11) and  $P_t$  is the thermal part of the first Piola–Kirchoff stress from (12), where  $P = SF^T$ ,  $\rho_0$  is the material density in the undeformed configuration,  $\ddot{u}$  is the acceleration, and  $F$  is the deformation gradient.

To develop the total lagrangian weak form for the momentum equation (34), we utilize the standard Galerkin approximation for both the displacement  $u$  and the test function  $\delta u$ , i.e.

$$u(X, t) = \mathbf{N}(X)\mathbf{u}(t), \tag{35}$$

and

$$\delta u(X, t) = \mathbf{N}(X)\delta\mathbf{u}(t), \tag{36}$$

where  $X$  specifies the material, or Lagrangian coordinates. Multiplying (34) by the test function  $\delta u$  and integrating over the domain gives

$$\int \delta u \left(\frac{dP_m}{dX} + \frac{dP_t}{dX} - \rho_0 \ddot{u}\right) dX = 0. \tag{37}$$

Performing the standard integration by parts, we obtain the final momentum equation weak form as

$$\begin{aligned} \delta\mathbf{u}^T \left(\int \rho_0 \mathbf{N}^T \mathbf{N} d\mathbf{X}\right) \ddot{\mathbf{u}} &= (\delta\mathbf{u}^T \mathbf{N}^T N^0 P_t)|_{r_0} \\ &+ (\delta\mathbf{u}^T \mathbf{N}^T N^0 P_m)|_{r_0} \\ &- \delta\mathbf{u}^T \left(\int \mathbf{B}^T P_m dX\right) \\ &- \delta\mathbf{u}^T \left(\int \mathbf{B}^T P_t dX\right), \end{aligned} \tag{38}$$

where  $N^0$  is unit normal in the undeformed configuration and  $\mathbf{B}$  is the derivative of the shape function vector, i.e.  $\mathbf{B} = \frac{d\mathbf{N}}{dX}$ . We assume that the thermal portion of the external force is zero, such that (38) can be written as

$$\mathbf{M}\ddot{\mathbf{u}} = \mathbf{f}_m^{\text{ext}} - \mathbf{f}_m^{\text{int}} - \mathbf{f}_t^{\text{int}}. \tag{39}$$

Again, we emphasize the coupling to the temperature field through the thermal part of the Piola–Kirchoff stress  $P_t$ .

#### 3.2. Heat equation weak form

The 1D heat equation can be written in Lagrangian form as

$$\frac{4k_B}{ha^3} \dot{T} - k \frac{\partial}{\partial X} \left(\frac{1}{F} \frac{\partial T}{\partial X}\right) + \frac{4k_B}{ha^3} \left(\frac{7D + 4E \cdot F^6}{D \cdot F + E \cdot F^7}\right) T \dot{F} = 0. \tag{40}$$

To derive the weak form for (40), we make the standard FE approximations for the temperature field:

$$T(\mathbf{X}, t) = \mathbf{N}(X)\mathbf{T}(t), \tag{41}$$

while the variations  $\delta T(X, t)$  follows the same interpolation as the temperature field that is defined in (41).

We first multiply Eq. (40) by the thermal test function  $\delta T$ , while integrating over the domain  $dX$  to give

$$\begin{aligned} \int \delta T \left(\frac{4k_B}{ha^3}\right) \frac{dT}{dt} dX &- \int \delta T k \frac{\partial}{\partial X} \left(\frac{1}{F} \frac{\partial T}{\partial X}\right) dX \\ &+ \int \delta T \left(\frac{4k_B}{ha^3}\right) \left(\frac{7D + 4E \cdot F^6}{D \cdot F + E \cdot F^7}\right) T \frac{dF}{dt} dX = 0. \end{aligned} \tag{42}$$

The final weak form for the heat equation can be written as

$$\begin{aligned} & \delta \mathbf{T}^T \left( \int \left( \frac{4k_B}{ha^3} \right) \mathbf{N}^T \mathbf{N} dX \right) \dot{\mathbf{T}} \\ & + \delta \mathbf{T}^T \left( \int \left( \frac{k}{F} \right) \mathbf{B}^T \mathbf{B} dX \right) \mathbf{T} \\ & + \delta \mathbf{T}^T \left( \int \left( \frac{4k_B}{ha^3} \right) \left( \frac{7D + 4E \cdot F^6}{D \cdot F + E \cdot F^7} \right) \frac{dF}{dt} \mathbf{N}^T \mathbf{N} dX \right) \mathbf{T} \\ & = \delta \mathbf{T}^T \left( \left( \frac{k}{F} \right) \mathbf{N}^T \mathbf{B} \mathbf{N}^0 \right) \Big|_{\Gamma_0} \mathbf{T}, \end{aligned} \quad (43)$$

or in more general form

$$\mathbf{M}_{TT} \dot{\mathbf{T}} + \mathbf{K}_{TT} \mathbf{T} + \mathbf{K}_{uT}(\dot{F}) \mathbf{T} = \mathbf{f}_T^{\text{ext}}, \quad (44)$$

where  $\mathbf{K}_{uT}$  is the thermomechanical coupling matrix.

## 4. Surface stress effects

### 4.1. A brief overview of surface stresses

Surface stresses constitute an important effect on the behavior and properties of nanomaterials, and arise in nanomaterials due to the fact that surface atoms have fewer bonding neighbors than those that lie within the material bulk. Consider the 1D atomic chain seen in Fig. 1 in which each atom interacts with both its nearest and next nearest neighbors. This interaction distance implies that atoms designated as bulk in Fig. 1 all have four bonding neighbors.

However, atoms at a free surface have fewer bonding neighbors. In this case, atom  $s_0$  has only three bonding neighbors, while atom  $s_1$  has only two. Because they have fewer bonding neighbors, these atoms are not at equilibrium, and relax to lower their potential energies. Another way of looking at this is that, in the initial undeformed configuration, the bulk atoms will each experience a zero net force. However, because the surface atoms do not have a full complement of bonding neighbors, they will each experience a non-zero net force in the undeformed initial configuration, which causes them to relax to find the minimum energy configuration of the 1D chain.

Surface stresses have been observed to be the cause for unique, non-bulk behavior and properties that have been observed in nanomaterials, including such phenomena as phase transformations, shape memory and pseudoelastic behavior [64–66]; further information on surface stress effects, their theoretical underpinnings and their effects on the behavior and properties of nanomaterials can be found in the excellent reviews of Cammarata [14] and Haiss [67].

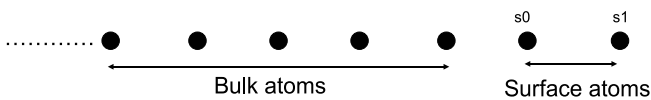


Fig. 1. Illustration of bulk and surface atoms in a 1D atomic chain.

### 4.2. 1D formulation

The incorporation of surface stress effects into the coupled thermomechanical formulation occurs through the modification of the Helmholtz free energy density in (8) following the surface Cauchy–Born (SCB) model developed by Park et al. [40,41]. We write the Helmholtz free energy in (8) corresponding to the 1D atomic chain visualized in Fig. 1 and thus incorporating surface effects as

$$\begin{aligned} A_{\text{total}} &= \int_{\Omega_0^{\text{bulk}}} \rho_0 \Psi_{\text{bulk}} d\Omega_0 + \int_{\Gamma_{s0}} \rho_0 \Psi_{s0} d\Gamma_{s0} \\ &+ \int_{\Gamma_{s1}} \rho_0 \Psi_{s1} d\Gamma_{s1}, \end{aligned} \quad (45)$$

where  $A_{\text{total}}$  is the total Helmholtz free energy of the system including both bulk and surface effects,  $\Psi_{\text{bulk}}$  is defined in (8), and the two surface Helmholtz free energy densities can be written as

$$\rho_0 \Psi_{s0} = \gamma_{s0}(\mathbf{C}) + nk_B \rho_{a0} T \ln \left( \frac{h \bar{D}_{s0}^{1/2n}(\mathbf{C})}{2\pi k_B T} \right), \quad (46)$$

$$\rho_0 \Psi_{s1} = \gamma_{s1}(\mathbf{C}) + nk_B \rho_{a1} T \ln \left( \frac{h \bar{D}_{s1}^{1/2n}(\mathbf{C})}{2\pi k_B T} \right), \quad (47)$$

where  $\rho_a$  is now the number of atoms per unit *area* of a given surface layer. The surface energy densities can be written as

$$\gamma_{s0} = \frac{1}{2} \frac{1}{\Gamma_0^{s0}} \sum_{i=1}^{n_{bs0}} U(r^{(i)}(\mathbf{C})), \quad (48)$$

$$\gamma_{s1} = \frac{1}{2} \frac{1}{\Gamma_0^{s1}} \sum_{i=1}^{n_{bs1}} U(r^{(i)}(\mathbf{C})), \quad (49)$$

where  $\Gamma_0^{s0}$  is the representative area for an atom in surface layer 0,  $\Gamma_0^{s1}$  is the representative area for an atom in surface layer 1,  $n_{bs0}$  is the number of bonds for an atom in surface layer 0 and  $n_{bs1}$  is the number of bonds for an atom in surface layer 1. Note that the surface energy densities are normalized by an *area* instead of a volume; this is necessary such that the surface energy densities scale correctly with changes in surface area to volume ratio as dictated by (45). Further details on the surface energy density and surface stresses can be found in Park et al. [40].

Upon obtaining the surface Helmholtz free energies in (46) and (47), the thermal and mechanical portions of the surface stress can be calculated as, following (10):

$$\mathbf{S}_m^{s1} = 2 \frac{\partial \gamma_{s1}(\mathbf{C})}{\partial \mathbf{C}} = \frac{1}{\Gamma_0^{s1}} \sum_{i=1}^{n_{bs1}} \left( U'(r^{(i)}) \frac{\partial r^{(i)}}{\partial \mathbf{C}} \right), \quad (50)$$

$$\mathbf{S}_m^{s0} = 2 \frac{\partial \gamma_{s0}(\mathbf{C})}{\partial \mathbf{C}} = \frac{1}{\Gamma_0^{s0}} \sum_{i=1}^{n_{bs0}} \left( U'(r^{(i)}) \frac{\partial r^{(i)}}{\partial \mathbf{C}} \right), \quad (51)$$

$$\mathbf{S}_t^{s1} = 2 \frac{\partial}{\partial \mathbf{C}} \left( nk_B \rho_{a1} T \ln \left( \frac{h \bar{D}_{s1}^{1/2n}(\mathbf{C})}{2\pi k_B T} \right) \right) = \frac{k_B \rho_{a1} T}{\bar{D}_{s1}} \frac{\partial \bar{D}_{s1}}{\partial \mathbf{C}}, \quad (52)$$

$$\mathbf{S}_t^{s0} = 2 \frac{\partial}{\partial \mathbf{C}} \left( nk_B \rho_{a0} T \ln \left( \frac{h \bar{D}_{s0}^{1/2n}(\mathbf{C})}{2\pi k_B T} \right) \right) = \frac{k_B \rho_{a0} T}{\bar{D}_{s0}} \frac{\partial \bar{D}_{s0}}{\partial \mathbf{C}}. \quad (53)$$

As can be seen in (50)–(53), the bulk and surface atoms have different values of mechanical stress due to the difference in the bulk energy density  $\Phi(\mathbf{C})$  and the surface energy density  $\gamma(\mathbf{C})$ . Furthermore, the bulk and surface atoms have different values of thermal stress, which occur because the values of the determinants of the surface dynamical matrices  $\bar{D}_s$  are different from those of the bulk atoms. Both of these scenarios are physically reasonable and meaningful, as these differences occur due to the fact that atoms at the surfaces of a nanostructure have a different bonding environment than do atoms in the bulk; these differences lead to different stress carrying capabilities and vibrational frequencies, leading to the difference in mechanical and thermal stresses between bulk and surface atoms.

### 4.3. Coupled equations including surface effects

The spatial decomposition of the bulk and non-bulk regions of the domain that result due to the consideration of surface stress effects is illustrated in Fig. 2. There, it is shown that the bulk region now covers the majority of the domain, except for a small region near the free surfaces. The size of the non-bulk region, in this case  $1.5h_a$ , where  $h_a$  is the lattice spacing, is dictated by the range of the interatomic potential, which in the present case extends to nearest and second nearest neighbor interactions.

The 1D mechanical weak form is modified due to the surface stresses to be

$$\begin{aligned} \delta \mathbf{u}^T \left( \int \rho_0 \mathbf{N}^T \mathbf{N} dX \right) \ddot{\mathbf{u}} &= (\delta \mathbf{u}^T \mathbf{N}^T N^0 P_t) |_{r_0} \\ &+ (\delta \mathbf{u}^T \mathbf{N}^T N^0 P_m) |_{r_0} \\ &- \delta \mathbf{u}^T \left( \int_{X_{0'}}^{X_{N'}} \frac{d\mathbf{N}^T}{dX} P_m dX \right) \\ &- \delta \mathbf{u}^T \left( \int_{X_{0'}}^{X_{N'}} \frac{d\mathbf{N}^T}{dX} P_t dX \right) \\ &- \delta \mathbf{u}^T \left( \frac{d\mathbf{N}^T}{dX} (P_m^{s0} + P_t^{s0}) \right) |_{r_{s0}} \\ &- \delta \mathbf{u}^T \left( \frac{d\mathbf{N}^T}{dX} (P_m^{s1} + P_t^{s1}) \right) |_{r_{s1}}. \quad (54) \end{aligned}$$

Note that while the bulk stresses are integrated over a volume (or the length  $dX$  in 1D), the surface stresses are integrated over an area. Because area degrades to a point in 1D, the integration is removed from the evaluation of the surface stresses in (54). The modified equation of motion can be written as

$$\mathbf{M}\ddot{\mathbf{u}} = \mathbf{f}_m^{\text{ext}} - \mathbf{f}_m^{\text{int}} - \mathbf{f}_t^{\text{int}} - \mathbf{f}_m^{s0} - \mathbf{f}_m^{s1} - \mathbf{f}_t^{s0} - \mathbf{f}_t^{s1}, \quad (55)$$

with the terms resulting from the surface stresses appearing as force vectors in the final equation of motion; note that these forces are non-zero only for elements that lie on the surfaces of the nanostructure.

The incorporation of surface stress effects also has similar effects on the weak form for the 1D heat equation, which takes the form

$$\begin{aligned} \delta \mathbf{T}^T \left( \int_{X_{0'}}^{X_{N'}} \left( \frac{4k_B}{ha^3} \right) \mathbf{N}^T \mathbf{N} dX + \frac{2k_B}{ha^2} \mathbf{N}^T \mathbf{N} |_{r_{s0}} + \frac{2k_B}{ha^2} \mathbf{N}^T \mathbf{N} |_{r_{s1}} \right) \dot{\mathbf{T}} \\ + \delta \mathbf{T}^T \left( \int \left( \frac{k}{F} \right) \mathbf{B}^T \mathbf{B} dX \right) \mathbf{T} \\ + \delta \mathbf{T}^T \left( \int_{X_{0'}}^{X_{N'}} \left( \frac{4k_B}{ha^3} \right) \left( \frac{7D + 4E \cdot F^6}{D \cdot F + E \cdot F^7} \right) \frac{dF}{dt} \mathbf{N}^T \mathbf{N} dX \right) \mathbf{T} \\ + \delta \mathbf{T}^T \left( \left( \frac{2k_B}{ha^2} \right) \left( \frac{7D_0 + 4E_0 \cdot F^6}{D_0 \cdot F + E_0 \cdot F^7} \right) \frac{dF}{dt} \mathbf{N}^T \mathbf{N} \right) |_{r_{s0}} \mathbf{T} \\ + \delta \mathbf{T}^T \left( \left( \frac{2k_B}{ha^2} \right) \left( \frac{7D_1 + 4E_1 \cdot F^6}{D_1 \cdot F + E_1 \cdot F^7} \right) \frac{dF}{dt} \mathbf{N}^T \mathbf{N} \right) |_{r_{s1}} \mathbf{T} \\ = \delta \mathbf{T}^T \left( \left( \frac{k}{F} \right) \mathbf{N}^T \mathbf{B} N^0 \right) |_{r_0} \mathbf{T}, \quad (56) \end{aligned}$$

where

$$\begin{aligned} D_0 &= \left( 2 + \frac{1}{2^{14}} \right) \frac{156\sigma^{12}}{ha^{14}}, \\ D_1 &= \left( 1 + \frac{1}{2^{14}} \right) \frac{156\sigma^{12}}{ha^{14}}, \\ E_0 &= - \left( 2 + \frac{1}{2^8} \right) \frac{42\sigma^6}{ha^8}, \\ E_1 &= - \left( 1 + \frac{1}{2^8} \right) \frac{42\sigma^6}{ha^8}. \end{aligned} \quad (57)$$

Eq. (56) can be written in a more general form as

$$(\mathbf{M}_{TT} + \mathbf{M}_{TT}^{s0} + \mathbf{M}_{TT}^{s1}) \dot{\mathbf{T}} + \mathbf{K}_{TT} \mathbf{T} + (\mathbf{K}_{uT} + \mathbf{K}_{uT}^{s0} + \mathbf{K}_{uT}^{s1}) \mathbf{T} = \mathbf{f}_T^{\text{ext}}. \quad (58)$$

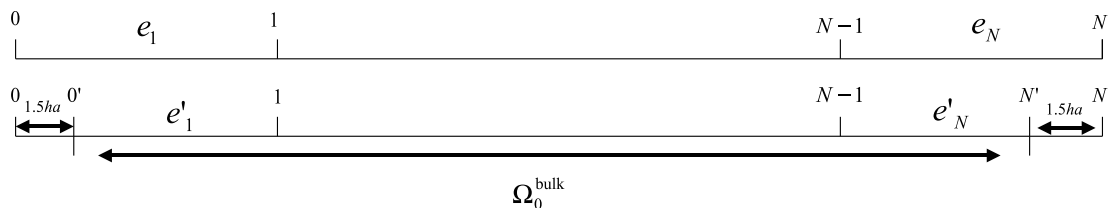


Fig. 2. Spatial decomposition of bulk and surface regions for FEM implementation of SCB model.

## 5. Fully implicit monolithic solution algorithm

As derived above, the FE discretization of the heat equation gives an equation of the form

$$\mathbf{M}_{TT}\dot{\mathbf{T}} + \mathbf{M}_{TT}^{\text{surf}}\dot{\mathbf{T}} + \mathbf{K}_{TT}\mathbf{T} + \mathbf{K}_{uT}(\dot{F})\mathbf{T} + \mathbf{K}_{uT}^{\text{surf}}\mathbf{T} = \mathbf{f}_T^{\text{ext}}, \quad (59)$$

where we have lumped all the surface stiffness terms in (58) into  $\mathbf{K}_{uT}^{\text{surf}}$  and all the surface mass terms in (58) into  $\mathbf{M}_{TT}^{\text{surf}}$  in (59).

Due to the tight, nonlinear coupling to the momentum equation in (59) through the  $\mathbf{K}_{uT}$  and  $\mathbf{K}_{uT}^{\text{surf}}$  terms, an exact solution to the coupled system of equations in (59) and (55) can be obtained through fully implicit monolithic solution in which the mechanical and thermal degrees of freedom are solved for simultaneously. One way to self-consistently solve the tightly coupled thermomechanical problem is to utilize the implicit, full Lagrangian approach of De and Aluru [49]. Following that approach, the FE discretized momentum equation (55) is solved using a Newmark scheme with an implicit trapezoidal rule, giving:

$$\mathbf{M}\ddot{\mathbf{u}}^{t+\Delta t} = \mathbf{f}_{\text{ext}}^{t+\Delta t} - \mathbf{f}_m^{t+\Delta t} - \mathbf{f}_t(\mathbf{T})^{t+\Delta t} - \mathbf{f}_{\text{surf}}^{t+\Delta t}, \quad (60)$$

$$\ddot{\mathbf{u}}^{t+\Delta t} = \frac{4}{\Delta t^2}(\mathbf{u}^{t+\Delta t} - \mathbf{u}^t - \dot{\mathbf{u}}^t \Delta t) - \ddot{\mathbf{u}}^t, \quad (61)$$

$$\dot{\mathbf{u}}^{t+\Delta t} = \dot{\mathbf{u}}^t + \frac{\Delta t}{2}(\ddot{\mathbf{u}}^t + \ddot{\mathbf{u}}^{t+\Delta t}), \quad (62)$$

where we have lumped all the forces due to surface stresses in (55) into  $\mathbf{f}_{\text{surf}}$  in (60). The temperature can then be updated using a backward Euler integrator as

$$\dot{\mathbf{T}}^{t+\Delta t} = \frac{1}{\Delta t}(\mathbf{T}^{t+\Delta t} - \mathbf{T}^t). \quad (63)$$

To self-consistently obtain the new displacement  $\mathbf{u}^{t+\Delta t}$  and the new temperature  $\mathbf{T}^{t+\Delta t}$ , we first obtain the mechanical residual  $\mathbf{R}_m$  and the thermal residual  $\mathbf{R}_t$  as

$$\mathbf{R}_m(\mathbf{u}, \mathbf{T}) = \mathbf{M}\ddot{\mathbf{u}} + \mathbf{f}_m^{\text{int}} + \mathbf{f}_t^{\text{int}}(\mathbf{T}) + \mathbf{f}_{\text{surf}} - \mathbf{f}_m^{\text{ext}}, \quad (64)$$

$$\mathbf{R}_t(\dot{\mathbf{u}}, \mathbf{T}) = \mathbf{M}_{TT}\dot{\mathbf{T}} + \mathbf{M}_{TT}^{\text{surf}}\dot{\mathbf{T}} + \mathbf{K}_{TT}\mathbf{T} + \mathbf{K}_{uT}\mathbf{T} + \mathbf{K}_{uT}^{\text{surf}}\mathbf{T} - \mathbf{f}_T^{\text{ext}}. \quad (65)$$

The matrix equation for the linearization of (64) and (65) giving the self-consistent solutions to  $\Delta \mathbf{T}$  and  $\Delta \mathbf{u}$  are written as

$$\begin{pmatrix} \frac{\partial \mathbf{R}_m}{\partial \mathbf{u}} & \frac{\partial \mathbf{R}_m}{\partial \mathbf{T}} \\ \frac{\partial \mathbf{R}_t}{\partial \mathbf{u}} & \frac{\partial \mathbf{R}_t}{\partial \mathbf{T}} \end{pmatrix} \begin{pmatrix} \Delta \mathbf{u} \\ \Delta \mathbf{T} \end{pmatrix} = - \begin{pmatrix} \mathbf{R}_m(\mathbf{u}, \mathbf{T}) \\ \mathbf{R}_t(\dot{\mathbf{u}}, \mathbf{T}) \end{pmatrix}. \quad (66)$$

Solving (66) iteratively until convergence of  $\Delta \mathbf{T}$  and  $\Delta \mathbf{u}$  gives the updated displacement  $\mathbf{u}^{t+\Delta t}$  and temperature  $\mathbf{T}^{t+\Delta t}$  accounting for the nonlinear coupling between the two variables of interest. After solving (66), the updated acceleration and velocity can be found from the new displacement via (61) and (62), while the updated rate of change of temperature can be found from (63).

Note that if surface stresses are not considered, the same algorithm can be used, while setting  $\mathbf{f}_{\text{surf}} = 0$  in (60) and  $\mathbf{K}_{uT}^{\text{surf}}$  and  $\mathbf{M}_{TT}^{\text{surf}}$  to be zero in (59).

## 6. Numerical examples

### 6.1. Verification: expansion of 1D chain due to surface stresses

We first verify the proposed approach by calculating the expansion of a 1D, 201 atom fixed/free atomic chain due to surface stresses, and in the absence of temperature. The chain was fixed at the left end, while the right end was free to move in response to both surface stresses. The equivalent SCB model was composed of 20 linear finite elements; for both simulations, the LJ potential parameters utilized were as follows:  $\sigma = 2.277 \text{ \AA}$ ,  $\epsilon = 6.649 \times 10^{-20} \text{ J}$ . Second nearest neighbor interactions were considered in the MD calculation, while the same interaction distance was utilized in setting up the bulk and surface unit cells for the SCB calculation.

This example is presented to illustrate the accuracy of the SCB model in capturing surface stresses within a dynamic formulation, and to set the stage for later verification examples illustrating that the inclusion of temperature, through the formulation presented within this work, leads to variations as compared to the 0 K case. It is first important to emphasize that if only first nearest neighbors are considered, the 1D chain does not deform because all atoms are in force equilibrium.

However, when second nearest neighbors are considered, there is a force imbalance on the surface atoms, and the 1D chain deforms accordingly. The comparison between the SCB end node displacement at the end atom displacement of the 1D chain are shown in Fig. 3; as can be seen, the SCB result matches the MD result. Thus, surface stress effects resulting from undercoordinated surface atoms are captured accurately using the SCB formulation in the absence of temperature.

### 6.2. Verification: thermal expansion of a 1D chain

We next verify that the proposed multiscale approach can accurately capture thermal expansion of a 1D chain at finite temperature. This is done by calculating the thermal expansion of a 1D, 201 atom fixed/free atomic chain that is identical to the example previously presented except that non-zero temperatures are now included in the formulation. The chain was fixed at the left end, while the right end was free to move in response to both surface stresses and thermal expansion. The equivalent SCB model was composed of 20 linear finite elements; for both simulations, the LJ potential parameters utilized were as follows:  $\sigma = 2.277 \text{ \AA}$ ,  $\epsilon = 6.649 \times 10^{-20} \text{ J}$ . Second nearest neighbor interactions were considered in the MD calculation, while the same interaction distance was utilized in setting up the bulk and surface unit cells for the SCB calculation.

The MD simulations were performed by constant temperature through usage of the Berendsen thermostat [68]; the Berendsen thermostat is implemented by rewriting the usual MD equation of motion in the following form:

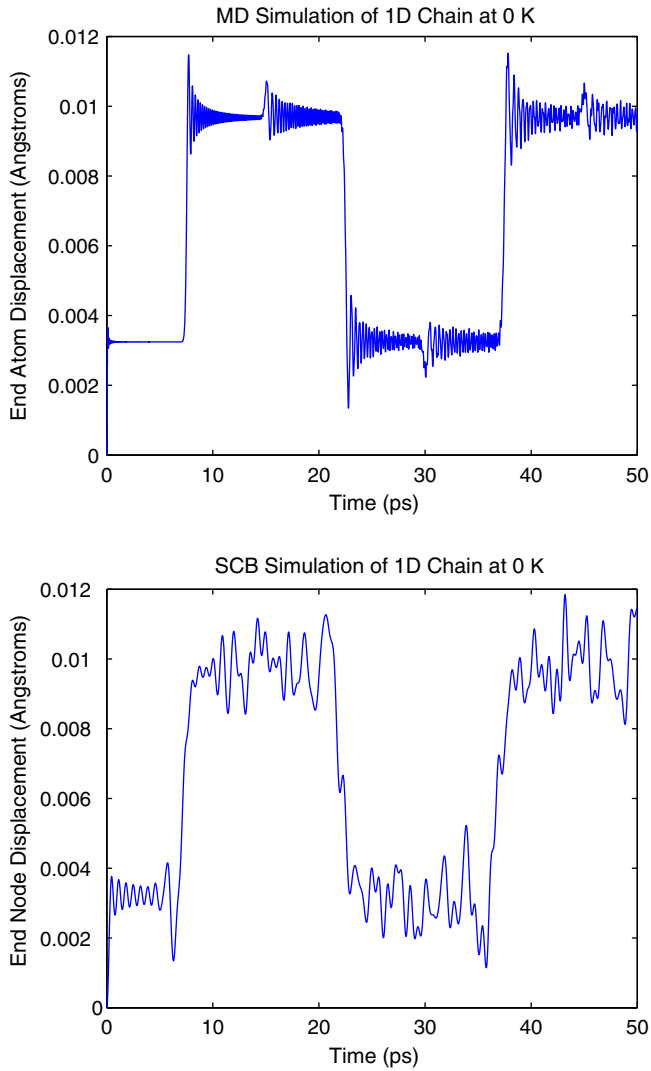


Fig. 3. Displacement time history of free end of 1D chain at 0 K.

$$m_i \dot{v}_i = F_i + m_i \gamma \left( \frac{T_0}{T} - 1 \right) v_i, \quad (67)$$

where  $\gamma$  is a friction coefficient,  $T_0$  is the target temperature for the MD system, and  $T$  is the current temperature. In the 1D MD simulations,  $\gamma$  was chosen to be  $0.025\sqrt{k/m}$ , or 2.5% of the atomic vibrational frequency. In the corresponding SCB calculations, the temperature was assumed to be uniform throughout the domain, and corresponded to the  $T_0$  utilized for the MD calculations.

The results for the thermal expansion of the free end of the chain are seen in Fig. 4 for the temperature at 100 K, and in Fig. 5 for the 300 K case. There are common features for both temperatures, for example the fact that the MD results show greater numerical noise than the SCB results; this is due to the fact that an implicit time integration algorithm, as described in the previous section, was used for the SCB calculation while an explicit, velocity Verlet algorithm was used for the MD simulations.

Despite the numerical noise, it is clear that for both temperatures, the vibrational period for the 1D chain is the

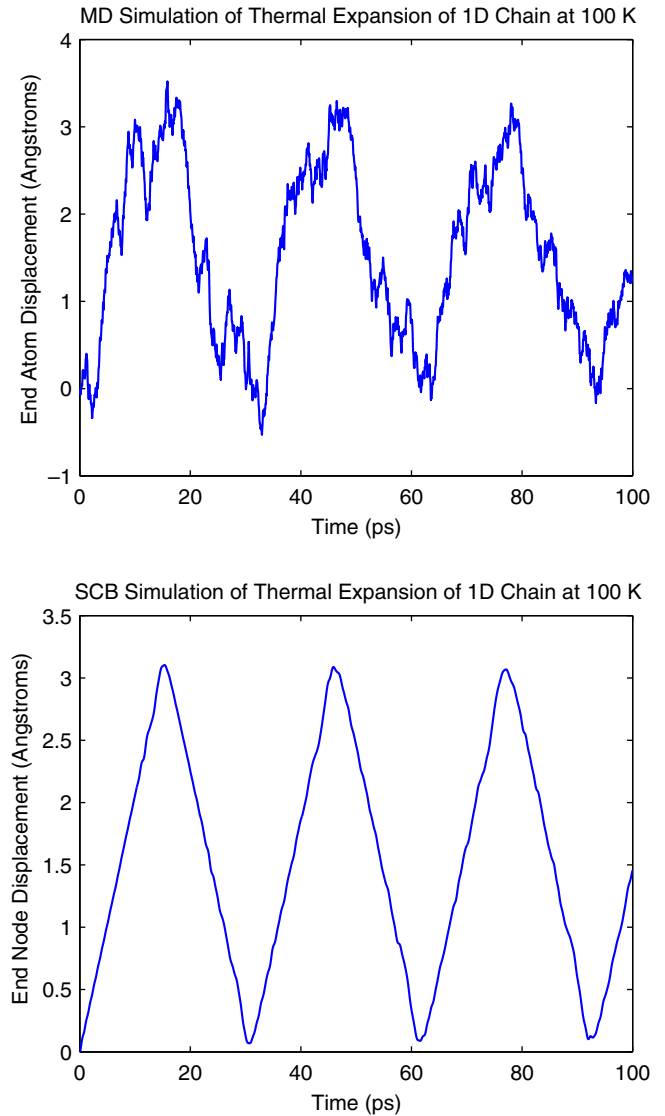


Fig. 4. Displacement time history of free end of 1D chain at 100 K.

same for both the MD and SCB calculations, with the peaks and valleys occurring at the same times in both simulations. Furthermore, for both temperatures, the SCB calculation captures the amplitude of the chain expansion (about 3.2 Å for the 100 K case, about 11 Å in the 300 K case) correctly, while also correctly predicting the increase in thermal expansion at the elevated temperature. We note that the thermal expansion is not a linear function of temperature due to the nonlinearity of the LJ potential, which is captured in the SCB calculation. Finally, the SCB calculation also captures the increase in vibrational period at elevated temperatures due to the larger thermal expansion of the free end.

### 6.3. 1D thermoelastic vibration

We consider a 1D thermoelastic vibration problem, which consists of the following boundary conditions [69]:

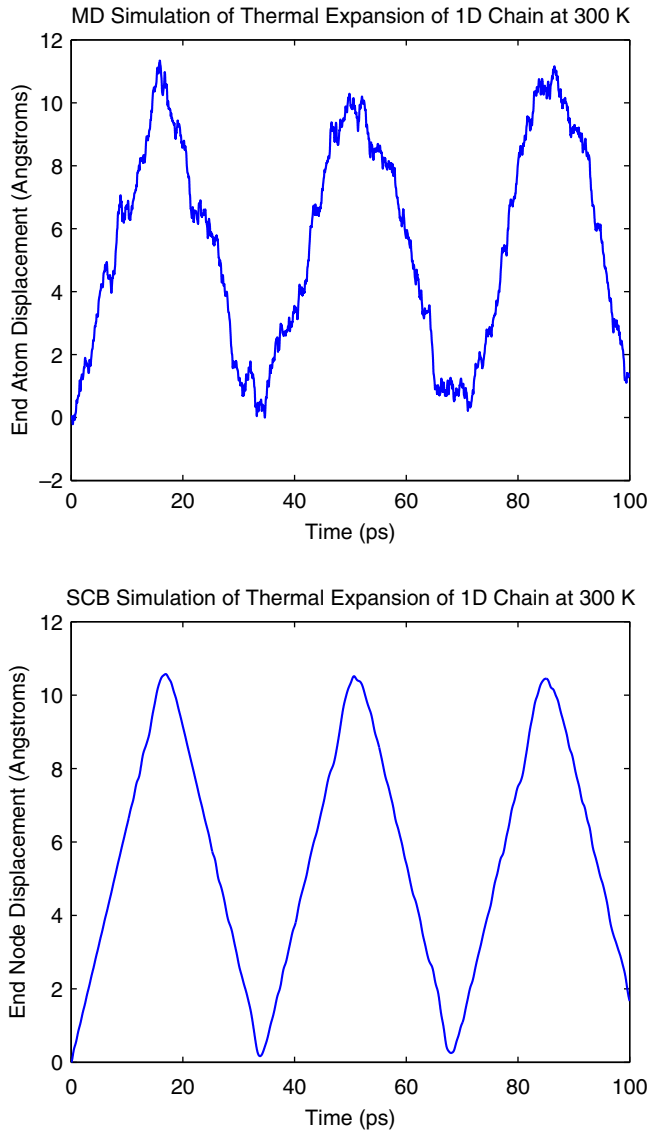


Fig. 5. Displacement time history of free end of 1D chain at 300 K.

strain of 1% at the chain center is designed to test the finite deformation formulation presented in this work. The problem was solved both the bulk Cauchy–Born (BCB) model, which neglects surface stress effects, as well as the current finite temperature surface Cauchy–Born (SCB) model to delineate the effects of surface stresses in a simple 1D setting.

The LJ potential parameters utilized were as follows:  $\sigma = 2.277 \text{ \AA}$ ,  $\epsilon = 6.649 \times 10^{-20} \text{ J}$ . These potential parameters led to a domain of length  $L = 511.17 \text{ \AA}$ , which was discretized using 100 linear finite elements and solved using the monolithic approach with a time step of  $\Delta t = 1.3 \times 10^{-4} \text{ ns}$ .

The BCB and SCB results for temperature and displacement are given in Figs. 6–8. The displacement shown in Fig. 6 is a time history of the displacement at the center of the 1D bar, and we make the following observations. First, note that the maximum magnitude of the displacement is  $0.025 \text{ \AA}$ , which is 1% of the lattice spacing, and thus

$$u(0, t) = u(L, t) = 0, \quad T(0, t) = T(L, t) = 298, \quad (68)$$

along with the initial conditions

$$u(x, 0) = 0, \quad v(x, 0) = \sin\left(\frac{\pi}{L}(x - x_0)\right), \quad T(x, 0) = 298, \quad (69)$$

where  $x_0$  is the coordinate of the left-hand side of the 1D chain.

The problem considered amounts to a 1D bar that is fixed at both ends and is prescribed a temperature of 298 K at the ends. The initial conditions are a constant temperature in the bar interior of 298 K, and an initial velocity in the form of a sine wave that has a maximum value at the center of the bar  $x = L/2$ , and decays to zero at the boundaries. The amplitude of the velocity sine wave was chosen such that the maximum displacement amplitude at the center of the 1D chain would be  $0.025 \text{ \AA}$ , which is 1% of the equilibrium lattice spacing; the maximum

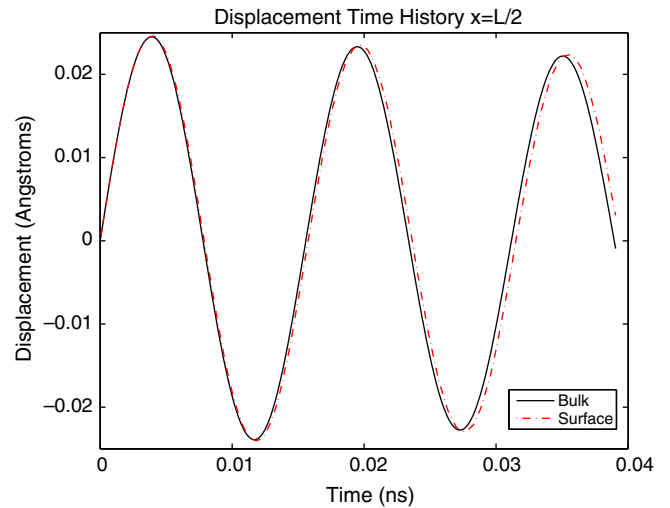


Fig. 6. Displacement time history at bar center for bulk and surface Cauchy–Born systems.

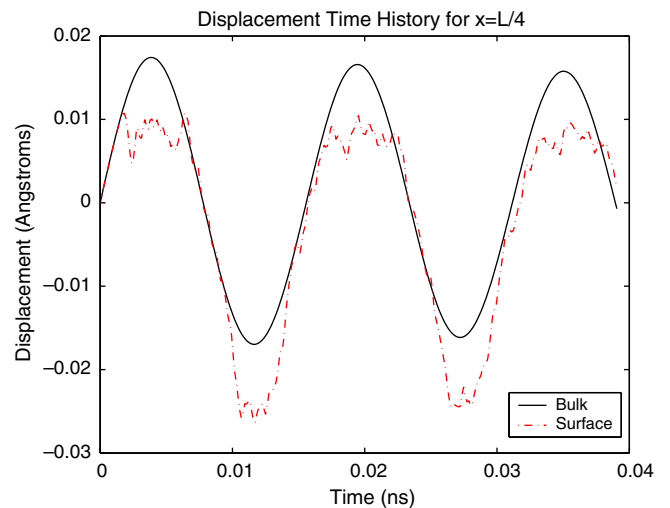


Fig. 7. Displacement time history at bar quarter point for bulk and surface Cauchy–Born systems.

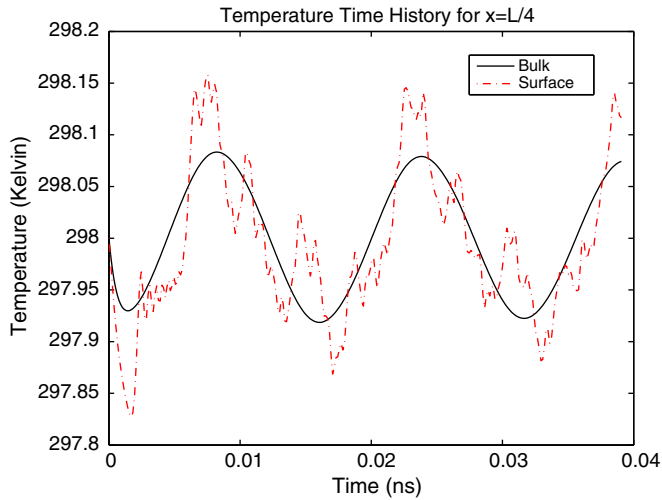


Fig. 8. Temperature time history at bar quarter point for bulk and surface Cauchy–Born systems.

constitutes a finite strain of 1% as previously discussed. Second, there is a distinct pattern of decrease in the displacement amplitude for both the BCB and SCB results over time, which occurs due to the fact that the simulations occurs at finite temperature; a value of 0 K for the temperature would result in no observed dissipation. While the BCB and SCB displacement histories at the bar center match closely, we observe a slight elongation of the oscillation period for the SCB case.

A greater disparity between the BCB and SCB results is observed when tracking the displacement time histories at the quarter point of the bar, or  $x = L/4$ , as seen in Fig. 7. First, it is noted that the displacement history for the BCB case is symmetric with time, or oscillates about zero displacement, with dissipation due to the thermoelastic coupling. Interestingly, the surface stresses clearly cause the SCB displacement history to be asymmetric as observed in Fig. 7. This asymmetry is not observed in Fig. 6 because the surface stress effects are cancelled at the bar center.

A comparison of the temperature at  $x = L/4$  is shown in Fig. 8. The BCB result is as expected; the temperature oscillates around the prescribed initial value of 298 K as the amplitude of the oscillations decrease due to the thermoelastic dissipation. However, the temperature profile for the SCB case is clearly different. First, the temperature profile is extremely rough. Second, the temperature increase that is observed in the SCB case clearly exceeds that seen in the BCB results.

The reason this occurs can be observed by analyzing the temperature time history. Note that the SCB temperature history initially tracks the BCB temperature history in Fig. 8. However, around a time of 0.002 ns, the SCB temperature history begins to diverge from the BCB temperature history, as a rapid temperature decrease is observed. This decrease in temperature corresponds to the time at which the deformation caused by the surface stresses has propagated in from the surface and reached the point

$x = L/4$ ; this time of departure (0.002 ns) between the BCB and SCB results is also observed in the displacement history at  $x = L/4$  in Fig. 7. Note that the time of maximum temperature (around 0.01 ns) in Fig. 8 occurs slightly before the time of minimum displacement in Fig. 7 suggesting the strong thermomechanical coupling that is present in the system.

We make one final important observation regarding surface stress effects on the thermomechanical behavior of nanomaterials based on the results shown in Figs. 9–11, which show the complete displacement and temperature histories for the bar center point and quarter point respectively. As can be seen in Fig. 9, the bar midpoint displacement history does not appear to change appreciably if surface stress effects are considered as the midpoint is a point of symmetry for the bar.

In contrast, the bar quarter point displacement histories are shown in Fig. 10, where a noticeable difference due to surface stresses can be observed, as may have been predicted based on the results of Fig. 7. In the BCB case,

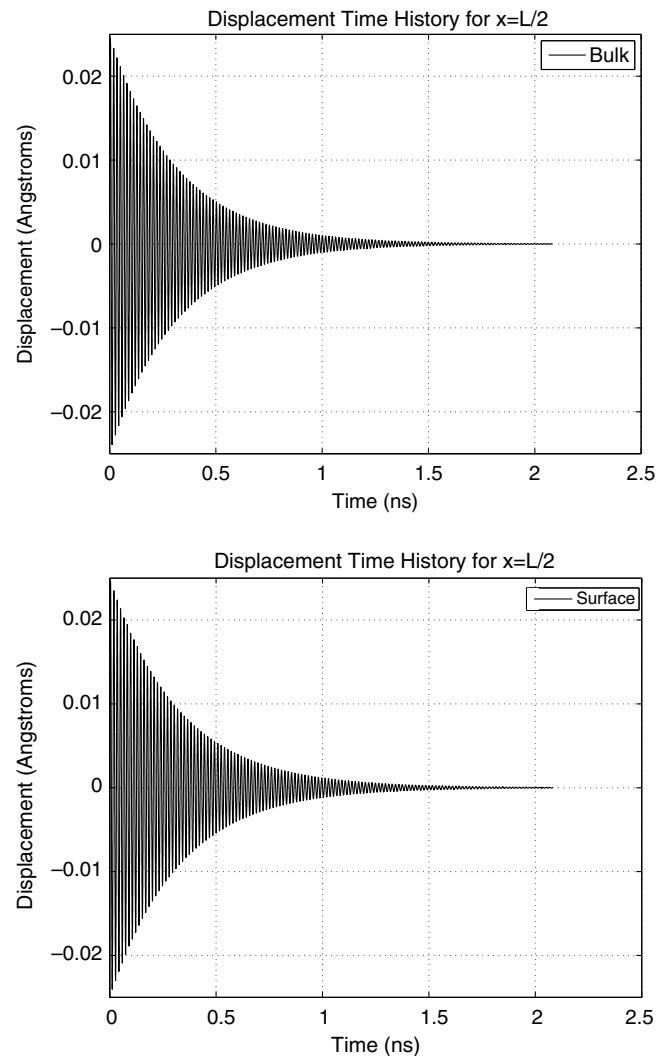


Fig. 9. Complete displacement time history at bar center for (top) bulk and (bottom) surface Cauchy–Born systems.

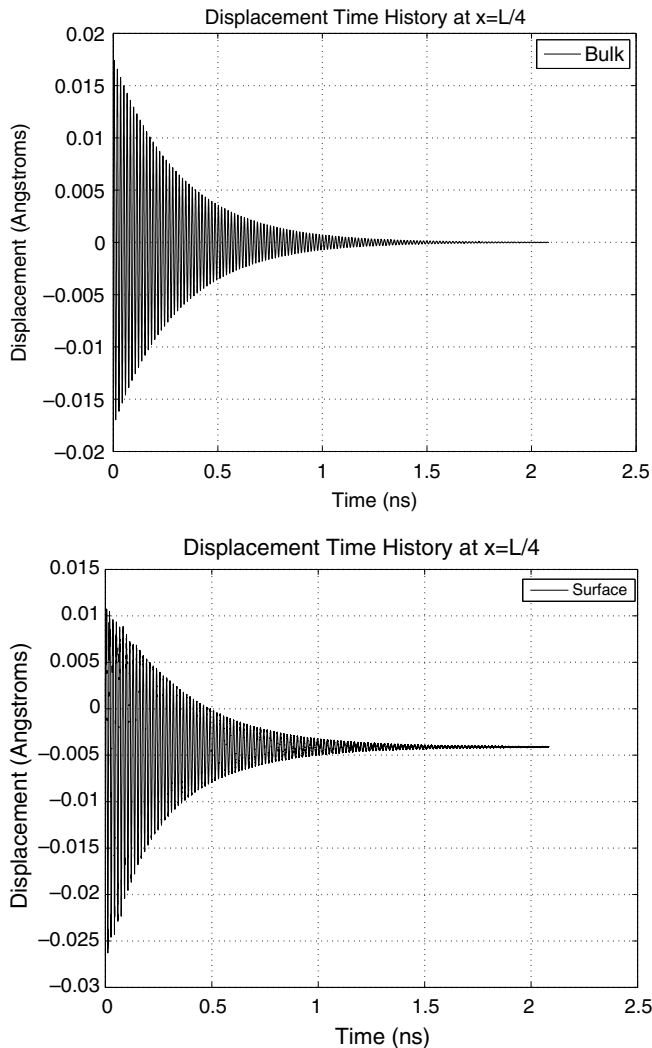


Fig. 10. Complete displacement time history at bar quarter point for (top) bulk and (bottom) surface Cauchy–Born systems.

the displacement oscillations decay to an essentially zero value over the course of time due to the thermomechanically-driven dissipation. In the SCB case, it is also observed that the displacement oscillations do decay in magnitude; however, the displacement of the bar quarter point in the SCB case never decays to zero.

This unusual thermomechanical behavior results from the fact that the surface stress effects are not diminished because the surface atoms are perpetually undercoordinated; this occurs because the ends of the bar are both fixed in this 1D example, and thus the surface atoms are not allowed to move to find their minimum energy configurations, as would occur if one of the ends of the bar were free [41]. Because of this and because the finite temperature causes thermal expansion of the bar, the final displacements of the left side of the bar ( $x < L/2$ ) are negative, while the final displacements on the right side of the bar ( $x > L/2$ ) are positive.

The effect of the bar quarter point displacement on the temperature is observed in Fig. 11; the temperature in both

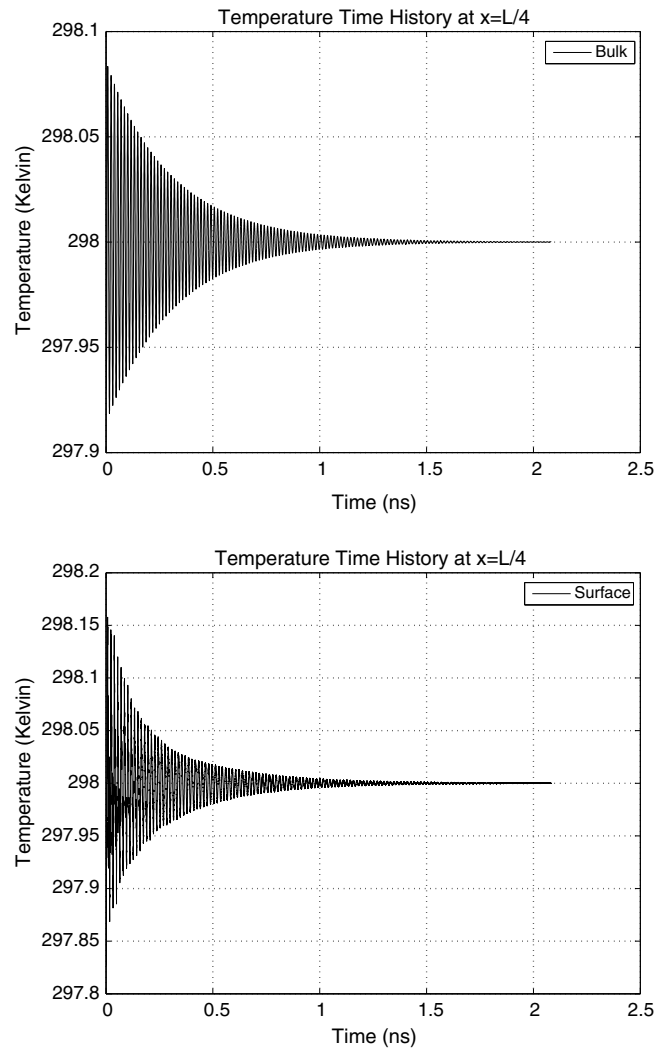


Fig. 11. Complete temperature time history at bar quarter point for (top) bulk system and (bottom) surface Cauchy–Born systems.

the BCB and SCB cases decays to the initial value of 298 K over the course of time. More interestingly, the thermal oscillations are observed to decay slightly faster in the SCB case. This occurs due to the fact that the mean displacement of the bar quarter point is not zero, as it is in the bulk case. This non-zero mean displacement thus drives a stronger coupling to the thermal field, and results in the increased dissipation in the SCB case as seen in Fig. 11.

## 7. Conclusion

In conclusion, we have presented a multiscale, finite deformation formulation for the thermoelastic analysis of nanomaterials. The analysis differs from previous approaches in that surface stress effects on the dynamic, thermoelastic behavior are fully accounted for through an extension to the previously developed surface Cauchy–Born model. The key to the proposed approach is the development of appropriate Helmholtz free energy representations for the bulk and surface atoms, which leads naturally to

the derivation of the modified momentum and heat equations that correctly account for surface stress effects and thus size-dependence on the thermoelastic behavior and properties of nanomaterials.

We first verified the method by calculating the thermal expansion of a fixed/free 1D atomic chain; the SCB model correctly predicted the vibrational periods, and the increase in thermal expansion at elevated temperatures. The SCB model was then utilized to illustrate that surface stresses have a strong impact on the thermomechanical behavior of nanomaterials. The displacement and temperature profiles of a 1D bar including surface stress effects were observed to vary markedly from that of a 1D bar modeled as a bulk material neglecting surface effects. We note that because the Lennard–Jones potential we have utilized in this work greatly underpredicts the values of surface stresses, the effects of surface stresses are expected to be significant in 3D nanosystems such as nanowires if realistic interatomic potentials such as the embedded atom method are utilized. We are currently pursuing this line of research.

### Acknowledgements

The authors acknowledge startup funding from Vanderbilt University in support of this research. H.S.P. also thanks Prof. Shaoping Xiao for sharing his time and code on the Helmholtz free energy, and Dr. Jonathan Zimmerman for helpful discussions.

### References

- [1] C.M. Lieber, Nanoscale science and technology: building a big future from small things, *MRS Bull.* 28 (7) (2003) 486–491.
- [2] P. Yang, The chemistry and physics of semiconductor nanowires, *MRS Bull.* 30 (2) (2005) 85–91.
- [3] Y. Xia, P. Yang, Y. Sun, Y. Wu, B. Mayers, B. Gates, Y. Yin, F. Kim, H. Yan, One-dimensional nanostructures: synthesis, characterization, and applications, *Adv. Mater.* 15 (5) (2003) 353–389.
- [4] H.G. Craighead, Nanoelectromechanical systems, *Science* 290 (2000) 1532–1535.
- [5] N.V. Lavrik, M.J. Sepaniak, P.G. Datskos, Cantilever transducers as a platform for chemical and biological sensors, *Rev. Sci. Instrum.* 75 (7) (2004) 2229–2253.
- [6] K.L. Ekinci, Electromechanical transducers at the nanoscale: actuation and sensing of motion in nanoelectromechanical systems (NEMS), *Small* 1 (8–9) (2005) 786–797.
- [7] J. Lou, L. Tong, Z. Ye, Modeling of silica nanowires for optical sensing, *Opt. Exp.* 13 (6) (2005) 2135–2140.
- [8] Y. Cui, Q. Wei, H. Park, C.M. Lieber, Nanowire nanosensors for highly sensitive and selective detection of biological and chemical species, *Science* 293 (2001) 1289–1292.
- [9] M.L. Roukes, Nanomechanical systems face the future, *Phys. World* 14 (2001) 25.
- [10] L.G. Zhou, H. Huang, Are surfaces elastically softer or stiffer? *Appl. Phys. Lett.* 84 (11) (2004) 1940–1942.
- [11] L.T. Canham, Silicon quantum wire array fabricated by electrochemical and chemical dissolution of wafers, *Appl. Phys. Lett.* 57 (10) (1990) 1046–1048.
- [12] D. Li, Y. Wu, P. Kim, L. Shi, P. Yang, A. Majumdar, Thermal conductivity of individual silicon nanowires, *Appl. Phys. Lett.* 83 (14) (2003) 2934–2936.
- [13] S. Pathak, V.B. Shenoy, Size dependence of thermal expansion of nanostructures, *Phys. Rev. B* 72 (2005) 113404.
- [14] R.C. Cammarata, Surface and interface stress effects in thin films, *Prog. Surf. Sci.* 46 (1) (1994) 1–38.
- [15] E.W. Wong, P.E. Sheehan, C.M. Lieber, Nanobeam mechanics: elasticity, strength, and toughness of nanorods and nanotubes, *Science* 277 (1997) 1971–1975.
- [16] S. Cuenot, C. Frétiigny, S. Demoustier-Champagne, B. Nysten, Surface tension effect on the mechanical properties of nanomaterials measured by atomic force microscopy, *Phys. Rev. B* 69 (2004) 165410.
- [17] B. Wu, A. Heidelberg, J.J. Boland, Mechanical properties of ultrahigh-strength gold nanowires, *Nat. Mater.* 4 (2005) 525–529.
- [18] G.Y. Jing, H.L. Duan, X.M. Sun, Z.S. Zhang, J. Xu, Y.D. Li, J.X. Wang, D.P. Yu, Surface effects on elastic properties of silver nanowires: contact atomic-force microscopy, *Phys. Rev. B* 73 (2006) 235409.
- [19] H. Liang, M. Upmanyu, H. Huang, Size-dependent elasticity of nanowires: nonlinear effects, *Phys. Rev. B* 71 (2005), 241403(R).
- [20] C. Ji, H.S. Park, Characterizing the elasticity of hollow metal nanowires, *Nanotechnology* 18 (2007) 115707.
- [21] M.E. Gurtin, A. Murdoch, A continuum theory of elastic material surfaces, *Arch. Ration. Mech. Anal.* 57 (1975) 291–323.
- [22] R.E. Miller, V.B. Shenoy, Size-dependent elastic properties of nanosized structural elements, *Nanotechnology* 11 (2000) 139–147.
- [23] V.B. Shenoy, Atomistic calculations of elastic properties of metallic FCC crystal surfaces, *Phys. Rev. B* 71 (2005) 094104.
- [24] P. Sharma, S. Ganti, N. Bhate, Effect of surfaces on the size-dependent elastic state of nano-inhomogeneities, *Appl. Phys. Lett.* 82 (4) (2003) 535–537.
- [25] C.T. Sun, H. Zhang, Size-dependent elastic moduli of platelike nanomaterials, *J. Appl. Phys.* 92 (2) (2003) 1212–1218.
- [26] R. Dingreville, J. Qu, M. Cherkaoui, Surface free energy and its effect on the elastic behavior of nano-sized particles, wires and films, *J. Mech. Phys. Solid* 53 (2005) 1827–1854.
- [27] J. Wang, H.L. Duan, Z.P. Huang, B.L. Karihaloo, A scaling law for properties of nano-structured materials, *Proc. Royal Soc. A* 462 (2006) 1355–1363.
- [28] J.-G. Guo, Y.-P. Zhao, The size-dependent elastic properties of nanofilms with surface effects, *J. Appl. Phys.* 98 (2005) 074306.
- [29] E. Tadmor, M. Ortiz, R. Phillips, Quasicontinuum analysis of defects in solids, *Philos. Mag. A* 73 (1996) 1529–1563.
- [30] L.E. Shilkrot, R.E. Miller, W.A. Curtin, Multiscale plasticity modeling: coupled atomistics and discrete dislocation mechanics, *J. Mech. Phys. Solid* 52 (2004) 755–787.
- [31] P.A. Klein, J.A. Zimmerman, Coupled atomistic-continuum simulation using arbitrary overlapping domains, *J. Comput. Phys.* 213 (2006) 86–116.
- [32] F.F. Abraham, J. Broughton, N. Bernstein, E. Kaxiras, Spanning the continuum to quantum length scales in a dynamic simulation of brittle fracture, *Europhys. Lett.* 44 (1998) 783–787.
- [33] R.E. Rudd, J.Q. Broughton, Coarse-grained molecular dynamics and the atomic limit of finite elements, *Phys. Rev. B* 58 (1998) 5893–5896.
- [34] W. E, Z.Y. Huang, A dynamic atomistic-continuum method for the simulation of crystalline materials, *J. Computat. Phys.* 182 (2002) 234–261.
- [35] G.J. Wagner, W.K. Liu, Coupling of atomistic and continuum simulations using a bridging scale decomposition, *J. Comput. Phys.* 190 (2003) 249–274.
- [36] H.S. Park, E.G. Karpov, W.K. Liu, P.A. Klein, The bridging scale for two-dimensional atomistic/continuum coupling, *Philos. Mag.* 85 (1) (2005) 79–113.
- [37] S.P. Xiao, T. Belytschko, A bridging domain method for coupling continua with molecular dynamics, *Comput. Methods Appl. Mech. Engrg.* 193 (2004) 1645–1669.
- [38] W.K. Liu, E.G. Karpov, H.S. Park, *Nano Mechanics and Materials: Theory, Multiscale Methods and Applications*, John Wiley and Sons, 2006.

- [39] G. Wei, Y. Shouwen, H. Ganyun, Finite element characterization of the size-dependent mechanical behaviour in nanosystems, *Nanotechnology* 17 (2006) 1118–1122.
- [40] H.S. Park, P.A. Klein, G.J. Wagner, A surface Cauchy–Born model for nanoscale materials, *Int. J. Numer. Methods Engrg.* 68 (2006) 1072–1095.
- [41] H.S. Park, P.A. Klein, Surface Cauchy–Born analysis of surface stress effects on metallic nanowires, *Phys. Rev. B* 75 (2007) 085408.
- [42] H.S. Park, P.A. Klein, Boundary condition and surface stress effects on the resonant properties of metal nanowires, *J. Mech. Phys. Solid*, submitted for publication.
- [43] G. Yun, H.S. Park, A finite element formulation for nanoscale resonant mass sensing using the surface Cauchy–Born model, *Comput. Methods Appl. Mech. Engrg.* 197 (2008) 3324–3336.
- [44] S. Xiao, W. Yang, Temperature-related Cauchy–Born rule for multiscale modeling of crystalline solids, *Computat. Mater. Sci.* 37 (2006) 374–379.
- [45] S. Xiao, W. Yang, A temperature-related homogenization technique and its implementation in the meshfree particle method for nanoscale simulations, *Int. J. Numer. Methods Engrg.* 69 (2007) 2099–2125.
- [46] X. Liu, S. Li, Nonequilibrium multiscale computational method, *J. Comput. Phys.* 126 (2007) 124105.
- [47] Z. Tang, H. Zhao, G. Li, N.R. Aluru, Finite-temperature quasicontinuum method for multiscale analysis of silicon nanostructures, *Phys. Rev. B* 74 (2006) 064110.
- [48] H. Zhao, Z. Tang, G. Li, N.R. Aluru, Quasiharmonic models for the calculation of thermodynamic properties of crystalline silicon under strain, *J. Appl. Phys.* 99 (2006) 064314.
- [49] S.K. De, N.R. Aluru, Theory of thermoelastic damping in electrostatically actuated microstructures, *Phys. Rev. B* 74 (2006) 144305.
- [50] P.A. Klein, A virtual internal bond approach to modeling crack nucleation and growth, Ph.D. Thesis, 1999, Stanford University.
- [51] M.S. Daw, M.I. Baskes, Embedded-atom method: derivation and application to impurities, surfaces, and other defects in metals, *Phys. Rev. B* 29 (12) (1984) 6443–6453.
- [52] E.B. Tadmor, G.S. Smith, N. Bernstein, E. Kaxiras, Mixed finite element and atomistic formulation for complex crystals, *Phys. Rev. B* 59 (1) (1999) 235–245.
- [53] H.S. Park, P.A. Klein, A surface Cauchy–Born model for silicon nanostructures, *Comput. Methods Appl. Mech. Engrg.* 197 (2008) 3249–3260.
- [54] P. Zhang, Y. Huang, P.H. Geubelle, P.A. Klein, K.C. Hwang, The elastic modulus of single-wall carbon nanotubes: a continuum analysis incorporating interatomic potentials, *Int. J. Solids Struct.* 39 (2002) 3893–3906.
- [55] M. Arroyo, T. Belytschko, An atomistic-based finite deformation membrane for single layer crystalline films, *J. Mech. Phys. Solid* 50 (2002) 1941–1977.
- [56] J.M. Rickman, R. LeSar, Free-energy calculations in materials research, *Ann. Rev. Mater. Res.* 32 (2002) 195–217.
- [57] R. LeSar, R. Najafabadi, D.J. Srolovitz, Finite-temperature defect properties from free-energy minimization, *Phys. Rev. Lett.* 63 (6) (1989) 624–627.
- [58] R. Najafabadi, D.J. Srolovitz, Evaluation of the accuracy of the free-energy-minimization method, *Phys. Rev. B* 52 (13) (1995) 9229–9241.
- [59] S.M. Foiles, Evaluation of harmonic methods for calculating the free energy of defects in solids, *Phys. Rev. B* 49 (21) (1994) 14930–14938.
- [60] A.N. Al-Rawi, A. Kara, P. Staikov, C. Ghosh, T.S. Rahman, Validity of the quasiharmonic analysis for surface thermal expansion of Ag (111), *Phys. Rev. Lett.* 86 (10) (2001) 2074–2077.
- [61] H. Parkus, Thermoelasticity, Blaisdell, 1968 (LCCN = 68-10326).
- [62] R. Lifshitz, M.L. Roukes, Thermoelastic damping in micro- and nanomechanical systems, *Phys. Rev. B* 61 (8) (2000) 5600–5609.
- [63] C. Zener, Internal friction in solids I: theory of internal friction in reeds, *Phys. Rev.* 52 (1937) 230–235.
- [64] J. Diao, K. Gall, M.L. Dunn, Surface-stress-induced phase transformation in metal nanowires, *Nat. Mater.* 2 (10) (2003) 656–660.
- [65] H.S. Park, K. Gall, J.A. Zimmerman, Shape memory and pseudoelasticity in metal nanowires, *Phys. Rev. Lett.* 95 (2005) 255504.
- [66] W. Liang, M. Zhou, F. Ke, Shape memory effect in Cu nanowires, *Nano Lett.* 5 (10) (2005) 2039–2043.
- [67] W. Haiss, Surface stress of clean and adsorbate-covered solids, *Rep. Prog. Phys.* 64 (2001) 591–648.
- [68] H.J.C. Berendsen, J.P.M. Postma, W.F.V. Gunsteren, A. DiNola, J.R. Haak, Molecular dynamics with coupling to an external bath, *J. Comput. Phys.* 81 (8) (1984) 3684–3690.
- [69] F. Armero, J.C. Simo, A new unconditionally stable fractional step method for non-linear coupled thermomechanical problems, *Int. J. Numer. Methods Engrg.* 35 (1992) 737–766.